

Disentangling spatio-temporal knowledge for weakly supervised object detection and segmentation in surgical video

Guiqiu Liao¹

Matjaz Jogan¹

Sai Koushik^{1,3}

Eric Eaton²

Daniel A. Hashimoto^{1,2}

¹Department of Surgery, University of Pennsylvania.

²Department of Computer and Information Science, University of Pennsylvania.

³Department of Electrical and Systems Engineering, University of Pennsylvania.

Abstract

Weakly supervised video object segmentation (WSVOS) enables the identification of segmentation maps without requiring an extensive training dataset of object masks, relying instead on coarse video labels indicating object presence. Current state-of-the-art methods either require multiple independent stages of processing that employ motion cues or, in the case of end-to-end trainable networks, lack in segmentation accuracy, in part due to the difficulty of learning segmentation maps from videos with transient object presence. This limits the application of WSVOS for semantic annotation of surgical videos where multiple surgical tools frequently move in and out of the field of view, a problem that is more difficult than typically encountered in WSVOS. This paper introduces Video Spatio-Temporal Disentanglement Networks (VDST-Net), a framework to disentangle spatiotemporal information using semi-decoupled knowledge distillation to predict high-quality class activation maps (CAMs). A teacher network designed to resolve temporal conflicts when specifics about object location and timing in the video are not provided works with a student network that integrates information over time by leveraging temporal dependencies. We demonstrate the efficacy of our framework on a public reference dataset and on a more challenging surgical video dataset where objects are, on average, present in less than 60% of annotated frames. Our method outperforms state-of-the-art techniques and generates superior segmentation masks under video-level weak supervision.

1. Introduction

Incorporating expert knowledge into machine learning for surgical video analysis demands extensive and costly

annotations. Annotated surgical video databases are rare but crucial for applications ranging from video review and analysis to AI supported robotic assistance [44].

The scarcity of annotated video is not unique to surgery. To address this, Weakly Supervised Semantic Segmentation (WSSS) methods were developed [7, 23, 25, 53], using image-level class labels to identify areas in an image that contain the corresponding object. Such methods have also been applied to video with frame-level labels, exploiting temporal information to improve accuracy [30, 32, 50].

In Weakly Supervised Video Object Segmentation (WSVOS), object labels are only available at video level, introducing uncertainty about object presence in each frame. Some approaches to WSVOS leverage motion cues [40, 51]. However, these methods often lack robustness against background motion and stationary objects. A recent end-to-end framework [1] has achieved state-of-the-art performance in object detection on two challenging datasets. In these datasets, the primary objects or concepts present in the video are labeled and are constantly present in most frames. We refer to this type of problem as Consistent Object Presence (COP), in contrast to Transient Object Presence (TOP) where no assumptions are made about object constancy (Figure 1). The latter case covers the significant variation in temporal presence of objects in surgical videos, where annotations are often based on the start and end times of surgical steps with annotated tools intermittently moving in and out of view. In Transient Object Presence (WSVOS-TOP), the algorithm must thus learn only from object classes without any implicit or explicit information on location, size, or temporal presence, and without assumptions about a specific count of object classes per frame.

In this work, we propose a method for WSVOS that addresses challenges with both COP and TOP problems. Our contributions include:

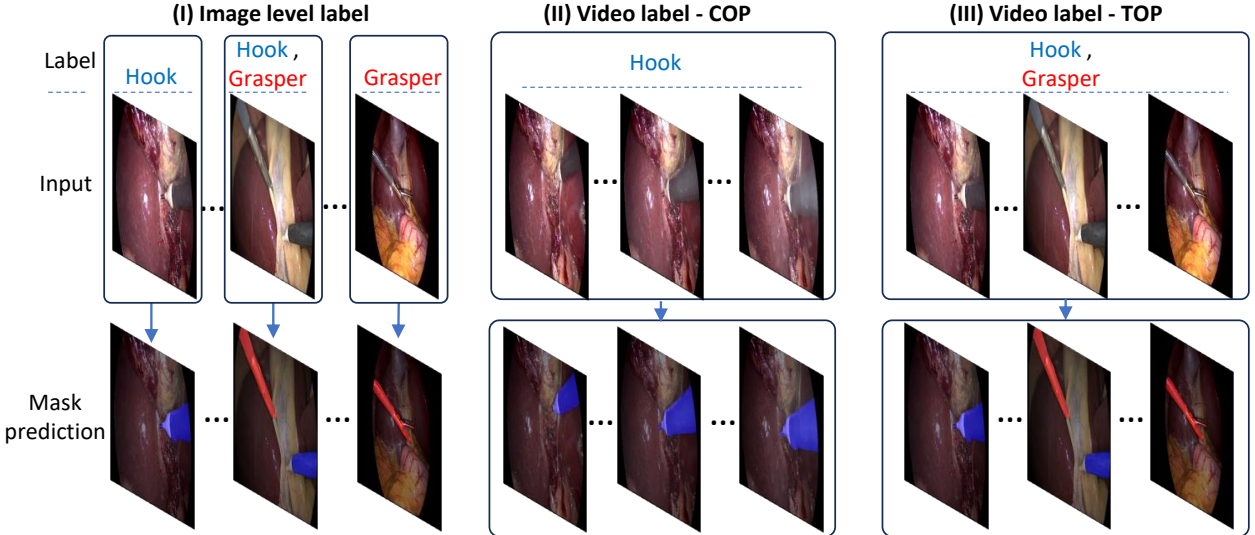


Figure 1. Three types of weakly supervised detection/segmentation in video. Type I has image-level presence labels available, and research for this task usually builds on WSSS adding temporal constraints to improve prediction. Type II WSVOS-COP only has video-level labels, and the object is assumed to be in the video for most of the frames (this is the scenario for YouTube-object dataset). Type III WSVOS-TOP is the most challenging, where the label only indicates the presence of objects for the whole video, yet each object may be present in the video temporarily (i.e., in only a subset of frames).

1. We propose an efficient network architecture to generate high-quality spatio-temporal class activation maps trained with video-level classification labels.
2. We introduce video spatio-temporal disentanglement networks (VDST-Net), which captures information associations across time and effectively addresses activation conflicts due to the complex interaction of multiple target objects, including objects appearing and disappearing from the video.
3. Experiments on YouTube-Objects (v2.2) demonstrate that our method outperforms state-of-the-art approaches in classic WSVOS-COP.
4. Experiments on our TOP surgical video dataset based on Cholec80 [43] with an average object presence rate of under 60% demonstrate a clear advantage of our method in WSVOS-TOP.

2. Related Work

2.1. Weakly supervised segmentation for image data

Image-level weakly supervised semantic segmentation has been well-researched, and most existing methods are based on Class Activation Map (CAM) [53]. Raw CAM may be sufficient for detection tasks, but it fails to delineate the target object at the semantic level as it tends to learn the most salient feature. Training strategies such as randomly masking out images [23] or feature maps [12, 26] can refine

the CAM by enhancing activation of novel features. Loss functions designed to improve CAM have been proposed, including SEC loss [21], CRF loss [37], regularization losses [49], and contrastive loss [48]. Recently, works on network modeling that explore the long-range dependence and attention mechanism of Vision Transformer (ViT) in CAM [7, 45] demonstrated ViT based CAM could outperform Convolutional Neural Networks (CNN) based models in image semantic segmentation tasks. There are emerging works that integrate foundation models with weakly supervised segmentation. [29] uses the Contrastive Language-Image Pretraining (CLIP) [34] for WSSS. Segment Anything Model (SAM) was also applied to WSSS [25]. While these methods improve segmentation performance for tasks with image-level labels, they are not directly applicable to weakly supervised segmentation tasks in video.

2.2. Weakly supervised detection and segmentation for video

Weakly supervised video segmentation can be categorized into three types of tasks, as shown in Figure 1. In the first type, frame-level object presence labels are provided. Research in this area often incorporates motion constraints to enhance prediction accuracy, as demonstrated in studies such as [27, 30, 50]. [32] employs LSTM to reason across time for detection and tracking in surgical videos. [13] adapts a 3D CNN to incorporate temporal dependencies for detection in videos. The second type of WSVOS

has object labels available only at the video-level, thus not explicitly determining object presence in a particular frame. However, an implicit assumption in the literature is that of a Consistent Object Presence (WSVOS-COP) setting, namely that the labeled objects are present throughout the video duration, treating occasional frames with missing objects as noise. This situation is exemplified by well-known reference datasets such as the YouTube-Objects datasets [17], which in addition contain only one object class per video. Consequently, this setup is close to a Type I problem as frame content can be inferred from video-level annotations. Recent work on TCAM [1] extracts the most reliable pseudo-semantic supervision signal in video to train a subsequent network for detection in individual images, efficiently addressing object detection for this case, while still showing limited robustness to smaller objects and temporal inconsistencies. In the third type (Type III), labels merely indicate the general presence of objects throughout an entire video, despite each object possibly appearing only temporarily. This is depicted in the right column of Figure 1. Consequently, the presence label assigned to a video may not accurately reflect a large subset of frames, introducing a significant challenge in learning generalized representations due to the increased uncertainty. Using motion cues could not resolve such an issue when including scenarios where the camera can occasionally move while the objects stay still. To the best of our knowledge, our work is the first to address this type of TOP data and train an end-to-end network to predict segmentation masks for the video as a whole.

2.3. Network reasoning across time and knowledge distillation

3D CNN [41], recurrent neural networks (RNN) [36], and temporal Transformers [47] are widely used architectures that capture time dependency and have been applied to various video and volumetric imaging tasks [28, 31, 54]. However, due to the lack of direct supervision signals, learning spatiotemporal features for weakly supervised segmentation is challenging. Knowledge Distillation (KD) [10] using a teacher-student network was originally designed for model compression and can gradually improve network learning capacity [6]. This property allows KD to enhance learning in weakly or semi-supervised tasks. L2G [14] applied KD to extend CAM from local to global. SCD [46] uses KD to incorporate feature correspondence for CAM refinement in images. Seco [48] employs KD to decouple occurrences for refining CAM in images. Our method employs KD to address the challenges posed by ill-posed video-level weak supervision, which causes activation conflicts leading to learning of features that are not associated with the correct class. We use a constrained teacher to allow the network not only to produce correct activation, but also

to refine the backbone to learn generalized features for new domain-specific data. Decoupled KD [52] has proven to be a versatile method for flexibly distilling meaningful knowledge. Our design, which could be categorized as being based on semi-decoupled KD, is tailored for video weakly supervised segmentation. Rather than relying on soft labels from the teacher, we enable the teacher’s predictions while utilizing ground truth to form gates for student supervision. This approach allows the student to learn effectively from an imperfect teacher while still gaining temporal reasoning abilities.

3. Methods

Figure 2 illustrates the proposed VDST-Net framework. The core of the framework consists of a teacher-student network pair designed to disentangle spatial and temporal knowledge. Both modules utilize a spatio-temporal class activation map (ST-CAM) and share input from a ViT [4]. The primary distinction between the teacher and student lies in their upper-layer feature extraction: the teacher employs a Multilayer Perceptron (MLP) module, while the student module uses a temporal convolutional network. This design constrains the teacher’s temporal interaction to overcome activation conflicts, while gradually increasing student’s learning capability to reason over time. We utilize a semi-decoupled distillation mechanism, supervising teacher and student models with identical video labels while enabling efficient knowledge transfer via gated activation maps. Despite the teacher’s powerful backbone and its ability to generate activation maps with a high degree of accuracy it still has detection gaps. Although the resulting supervision signal is not perfect, semi-decoupled distillation allows the student to use the teacher CAMs information efficiently while adding temporal context.

3.1. Video encoder

A ViT encoder is used to encode patches from individual frames of the input video $V \in \mathbb{R}^{W \times H \times D}$, producing a stack of token embeddings reshaped as $T \in \mathbb{R}^{w \times h \times D \times C_e}$, where $w = W/P$, $h = H/P$, and P denotes the width/height of a patch, and C_e is the embedding dimension. T captures features with strict temporal correspondence (maintaining the temporal dimension D) and high spatial correspondence.

3.2. Teacher module

T is further processed by a MLP block that linearly projects T to C channels of a feature map $F^t \in \mathbb{R}^{w \times h \times D \times C}$, maintaining spatio-temporal correspondence. Following a line of work on ViT-based 2D CAM [7, 45], spatial pooling is applied to F^t to obtain a slice-wise feature map $F_s^t \in \mathbb{R}^{1 \times 1 \times D \times C}$. Then temporal pooling is applied to acquire a final feature map for video classification

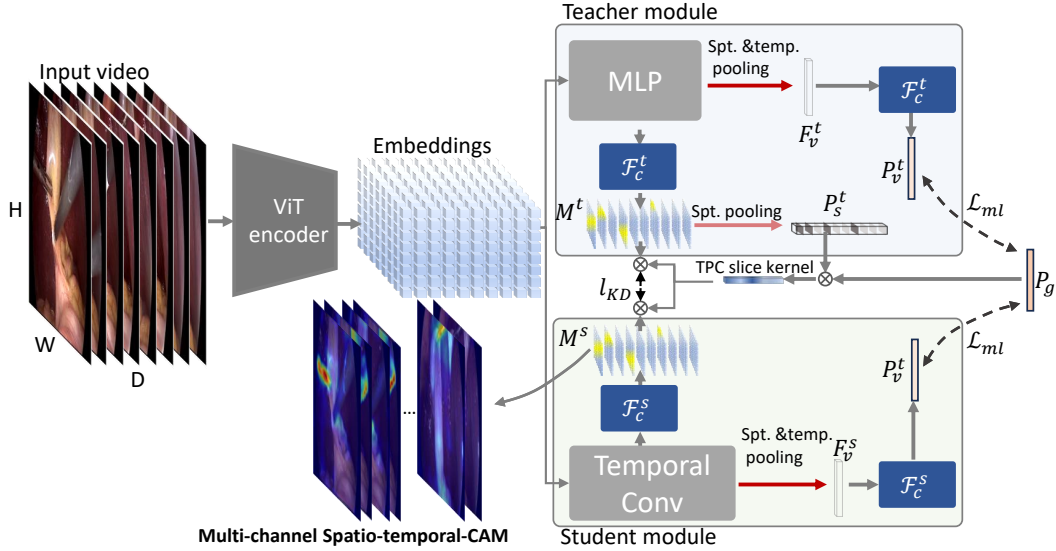


Figure 2. Our VDST-Net approach deploying knowledge distillation to disentangle spatial and temporal information for weakly supervised learning with video-level labels.

$F_v^t \in \mathbb{R}^{1 \times 1 \times 1 \times C}$. Inspired by weakly supervised temporal scene localization [38], a ranked top- k average pooling is adopted. This approach first ranks all the spatial patch features by magnitude, and then selects the top- k_1 patches for average pooling. Then ranked top- k_2 is applied to select the temporal feature. It balances between max pooling and average pooling; a fine-tuned optimal k -value could be correlated to object-to-background ratio and within-video object presence frequency. Finally, with a fully connected classification layer \mathcal{F}_c^t , the final video prediction $P_v^t \in \mathbb{R}^{1 \times 1 \times 1 \times N}$ is obtained by $P_v^t = \mathcal{F}_c^t(F_v^t)$, where N is the number of classes. Plugging \mathcal{F}_c^t channel-wise to feature map F^t results in a multi-channel ST-CAM $M^t \in \mathbb{R}^{w \times h \times D \times N}$.

3.3. Student module

Employing an MLP for encoding of embeddings T processes each frame in isolation, thus eliminating temporal conflicts. However, it fails to exploit temporal coherence to enhance prediction robustness. Temporal convolutional layers on the other hand can infer associations between frames, yet will introduce errors due to the absence of frame-level annotation. To mitigate this issue, we utilize a semi-decoupled KD technique that refines a student network with higher capacity through efficiently selected supervision signals. In this context, we designate a temporal convolution-based network as the student module. The student network adopts the same spatio-temporal pooling mechanism from the teacher and trains an additional fully connected classification layer \mathcal{F}_c^s . This layer produces the student's video prediction $P_v^s \in \mathbb{R}^{1 \times 1 \times 1 \times N}$ and the student

ST-CAM $M^s \in \mathbb{R}^{w \times h \times D \times N}$.

3.4. Semi-decoupled distillation and training loss

To help the backbone learn generalized features at different scales, features from each MLP layer in the teacher module are randomly downsampled during training with a probability of 0.5. Next, we employ a semi-decoupled [52] approach to knowledge distillation (KD), where we use video ground truth labels to supervise both teacher and student networks' predictions while applying KD on activation maps. The teacher module is trained solely on a multi-label soft margin classification loss $\mathcal{L}_{ml}(P_v^t, P_g)$ using ground truth video labels $P_g \in \mathbb{R}^{1 \times N}$. For the student module, in addition to the classification loss, we include a KD loss to further refine the student's activation map. This loss is computed by considering only the true positive channel (TPC) and positive slice predictions from the teacher network.

Initially, a teacher slice prediction $P_s^t \in \mathbb{R}^{1 \times 1 \times D \times N}$ is obtained by applying maximum spatial pooling to the teacher ST-CAM. Subsequently, we create a TPC slice kernel $K_{tp} \in \mathbb{R}^{1 \times 1 \times D \times N}$ through the operation $K_{tp} = P_s^t \otimes r(P_g)$, where $r(\cdot)$ represents a repeating operation to match dimensions for element-wise multiplication \otimes . A final gated KD loss is calculated by:

$$l_{KD} = \mathcal{L}_{mse}(M^s \otimes r(K_{tp}), M^t \otimes r(K_{tp})) , \quad (1)$$

where \mathcal{L}_{mse} is a Mean Squared Error loss function, and $r(\cdot)$ here matches the dimension of K_{tp} to M^t and M^s . In analogy, this operation resembles focusing exclusively on frames where true positive pseudo masks are predicted, akin to singling out specific instances for loss calculation. The

final loss used for optimizing the student module is given by:

$$l_s = \mathcal{L}_{ml}(P_v^s, P_g) + \alpha l_{KD} . \quad (2)$$

In Eq. (2) α is a scaling factor for the distillation loss. Finally, we apply a ReLU layer and normalization to the ST-CAMs extracted from classification networks.

4. Experiments

4.1. Datasets

To investigate the characteristics of our proposed method, we utilize two distinct video dataset collections: YouTube-Objects video dataset (v2.2) [17] and Cholec80 dataset [43]. YouTube-objects data contains 106 videos for training, and 49 videos for testing, where ten categories ($N = 10$) of objects are covered. Each video is split into short-duration clips, and in each clip a few frames are annotated with a bounding box for evaluation. The Cholec80 dataset consists of 80 cholecystectomy surgery videos, each downsampled to 1 FPS, with labels indicating the presence or absence of seven surgical tools ($N = 7$) in each frame. We create a variant TOP video dataset based on Cholec80. First these videos are split into 30-second clips without overlap, merging the tool labels across frames to generate a video-level tool presence binary vector label for each clip. The test set is based on CholecSeg8K [11] which contains 8K images from 17 videos in Cholec80 with segmentation labels for instruments and anatomy. From this dataset we derive 100 video clips containing 3K frames. To prevent contamination between testing and training data, 5,296 training clips are sampled from 63 Cholec80 videos not included in CholecSeg8K. We calculate the tool frequencies across clips using frame per clip (FPC) which denotes the percentage of frames in a clip with the tool present. YouTube-Objects dataset has nearly 100% FPC for each clip and thus represents the second case (Type II – WSVOS-COP) demonstrated in Figure 1. Most categories in Cholec80 based dataset appear on average in less than 60% of the frames of a particular video labeled with that category, which makes it a much more challenging dataset that represents a WSVOS-TOP (Type III) problem.

4.2. Experimental Setup and Evaluation Metrics

We refrained from data augmentation and present the results trained only with original images in this paper. Video frames were resized to 256×256 pixels. Adam optimizer with a learning rate of 1×10^{-4} and a weight decay of 1×10^{-4} was used for training. For the initial nine epochs, only the teacher module and backbone were optimized. Subsequently, the student module was activated alongside the teacher. The k_1 value is calculated as 10% of the number of patches. We fine-tune the k_2 value for the ranked-pooling based on data, and the final results reported in this paper are

under $k_2 = 67\%L_v$ (L_v is video length) for the YouTube-Objects data, and $k_2 = 40\%L_v$ for the surgical data. We assessed the classification accuracy on frame and video level. For all the models, final segmentations were refined using dense CRF [22]. For the surgical dataset, segmentation performance was evaluated using Intersection over Union (IoU), Dice score and Hausdorff distance (HD). For localization performance we use CorLoc (IoU > 50%) rate [1].

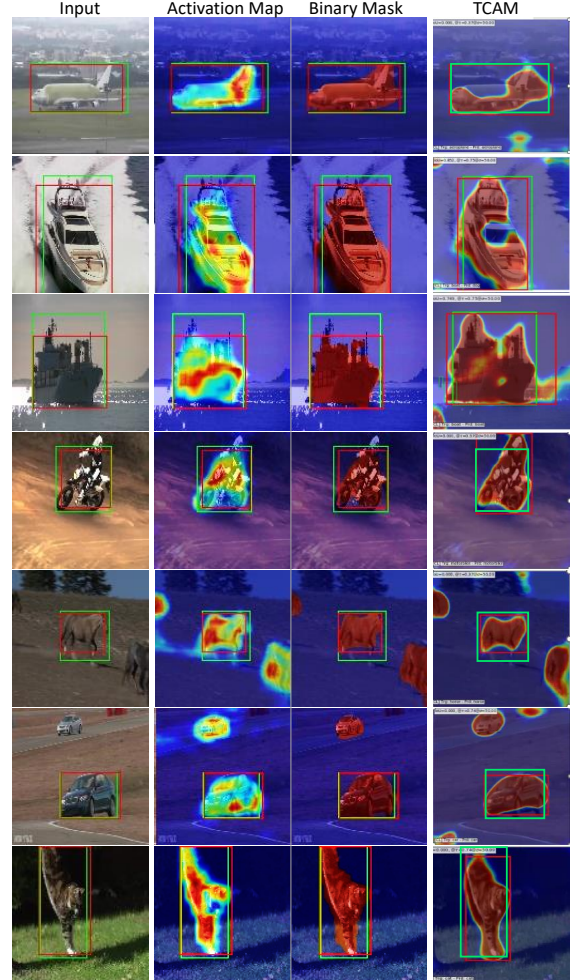


Figure 3. Segmentation and detection performance on YouTube Objects data. The second and third columns are the activation maps and post-processed binary masks of our method. In the last column results are taken from [1].

4.3. Analysis on YouTube video object detection Performance

As shown in Table 1, among state-of-the-art methods, TCAM [1] leads in performance on the YouTube-Objects dataset for localization. However, qualitatively, it tends to underfit the object contours and over-activate on background, resulting in lower segmentation quality compared

Table 1. Detection performance on YouTube-Objects [33] dataset under CorLoc Metrics.

Method	Aero	Bird	Boat	Car	Cat	Cow	Dog	Horse	Mbikes	Train	avg
(Joulin et al., 2014) [16]	25.1	31.2	27.8	38.5	41.2	28.4	33.9	35.6	23.1	25.0	31.0
(Kwak et al., 2015) [24]	56.5	66.4	58.0	76.8	39.9	69.3	50.4	56.3	53.0	31.0	55.8
(Rochan et al., 2016) [35]	60.8	54.6	34.7	57.4	19.2	42.1	35.8	30.4	11.7	11.4	35.8
(Tokmakov et al., 2016) [40]	71.5	74.0	44.8	72.3	52.0	46.4	71.9	54.6	45.9	32.1	56.6
(Koh et al., 2016) [20]	64.3	63.2	73.3	68.9	44.4	62.5	71.4	52.3	78.6	23.1	60.2
(Tsai et al., 2016) [42]	66.1	59.8	63.1	72.5	54.0	64.9	66.2	50.6	39.3	42.5	57.9
(Haller and Leordeanu, 2017) [8]	76.3	71.4	65.0	58.9	68.0	55.9	70.6	33.3	69.7	42.4	61.2
(Croitoru et al., 2019) [3]	81.7	51.5	54.1	62.5	49.7	68.8	55.9	50.4	33.3	57.0	56.5
XGradCAM(Fu et al., 2020) [5]	68.2	44.5	45.8	64.0	46.8	86.4	44.0	57.0	44.9	45.0	54.6
LayerCAM(Jiang et al., 2021) [15]	80.0	84.5	47.2	73.5	55.3	83.6	71.3	60.8	55.7	48.1	66.0
TCAM (Belharbi et al., 2023) [1]	79.4	94.9	75.7	61.7	68.8	87.1	75.0	62.4	72.1	45.0	72.2
VDST-Net + Res34 frozen	T only	70.6	97.8	44.7	78.0	31.3	57.7	53.8	42.5	73.9	15.6
	T-S fusion	81.6	97.7	74.4	73.9	66.7	71.4	71.8	51.6	59.5	25.0
	full	91.5	93.5	67.4	82.5	63.4	80.6	64.1	56.3	55.3	36.2
VDST-Net + Res34 refined by S	T only	88.0	95.7	74.6	69.7	78.5	80.7	57.1	62.4	55.8	20.9
	T-S fusion	87.7	95.1	76.1	70.5	81.6	81.2	58.7	61.3	58.0	22.9
	full	86.4	95.1	77.8	71.8	76.2	77.2	54.2	55.1	57.7	22.1
VDST-Net + Res34 refined by T	T only	86.1	94.3	75.6	72.9	76.7	76.2	57.9	60.4	61.6	23.1
	T-S fusion	90.0	93.3	77.2	71.8	84.8	80.7	60.9	68.8	58.6	36.4
	full	85.4	90.9	73.2	69.0	82.5	75.2	55.8	73.8	51.5	48.4
VDST-Net + DINO ViT (refined by T)	T only	83.8	88.6	69.5	59.3	80.7	76.6	43.2	64.9	48.7	17.8
	T-S fusion	91.0	88.2	72.7	68.7	85.9	79.2	52.4	70.4	55.9	37.0
	full	92.3	91.8	72.3	70.1	82.2	82.5	73.6	72.6	67.8	50.7

to our method, as illustrated in Figure 3. Our method achieves an overall accuracy improvement from 72.2% to 75.6%. Segmentation scores are not reported due to the lack of ground truth masks in the official dataset.

Our method is primarily designed for ViT-based feature extractors, utilizing the pre-trained DINO ViT [2] as our backbone and fine-tuning are on domain-specific data. We also measure performance using a ResNet34 backbone with our proposed spatio-temporal disentanglement methodology, by converting ResNet features to match the format produced by ViT. We investigate different optimization strategies for the backbone on new domain data: back-propagation through the teacher (denoted as “refined by T”), through the student (“refined by S”), or keeping the backbone frozen. Detection outputs from either Teacher (T) or final student (full) or extracted from fused CAM (T-S fusion) are presented. Our experiments show that even a completely frozen ResNet captures a certain level of generalized features. Through our semi-decoupled KD approach, we achieve a performance improvement from 56.6% to 69.1%. Interestingly, refining the backbone through the student tends to degrade the final output compared to MLP teacher (68.4% to 67.4%), likely due to the challenge of learning generalized features from video-level labels with higher uncertainty. Optimizing the backbone through the teacher proves to be the effective approach for both ResNet and ViT backbones, leading to a stronger student model by leveraging well-learned features. For ResNet, we observe that the T-S fusion has better bounding box localization than

final student (72.2% vs. 70.6%), possibly because ResNet features are less generalized and lean more toward the MLP from the teacher module, while the activations learned by the student complement those of the teacher. In conclusion, we recommend using ViT within our framework and advise against direct student-driven backbone refinements.

4.4. Surgical video tool segmentation performance

On surgical videos, we compare our method to frame-level weakly supervised methods MCTformer [45], LayerCAM [15], and XGradCAM [5], all trained with frame-level labels. Models were adapted to our dataset using their open-source code implementations. We also compare our method to the video-level supervised method TCAM [1], where both our method and TCAM are trained with more challenging video-level class labels. We test our model using teacher (T) only, teacher-student (T-S) fusion, and

Table 2. Comparison to state-of-the-art weakly supervised methods with either frame-level supervision or video-level supervision. Video (V) and Frame (F) accuracy (AC)

Method	V-AC[%] \uparrow	F-AC[%] \uparrow	IoU[%] \uparrow	HD[pixel] \downarrow
MCTformer [45]	98.27	97.63	43.14	50.07
LayerCAM [15]	95.67	94.87	31.97	75.59
XGradCAM [5]	92.21	90.21	32.13	53.53
TCAM [1]	97.08	95.10	28.22	54.60
T only (ours)	98.26	97.56	47.50	48.72
T-S fusion (ours)	97.11	97.23	48.64	39.61
VDST-Net (ours)	96.82	98.23	61.80	28.10

Table 3. Ablation study with modifications of overall architecture, spatio-temporal pooling and training strategies. W/O denotes a specific module is removed.

	Conditions	Video AC[%]↑	Frame AC[%]↑	IoU[%]↑	Dice[%]↑	HD[pixel]↓
	VDST-Net full	96.82	98.23	61.80	67.80	28.10
Structural ablation	Teacher only	98.41	97.56	47.50	53.07	48.72
	Student only	94.37	94.76	42.83	47.78	69.45
Training	Avg pooling	94.37	94.51	53.16	56.31	41.65
	Max strategy	94.95	95.19	52.47	56.09	40.05
	W/O TPC kernel	96.54	97.10	60.46	63.64	40.75

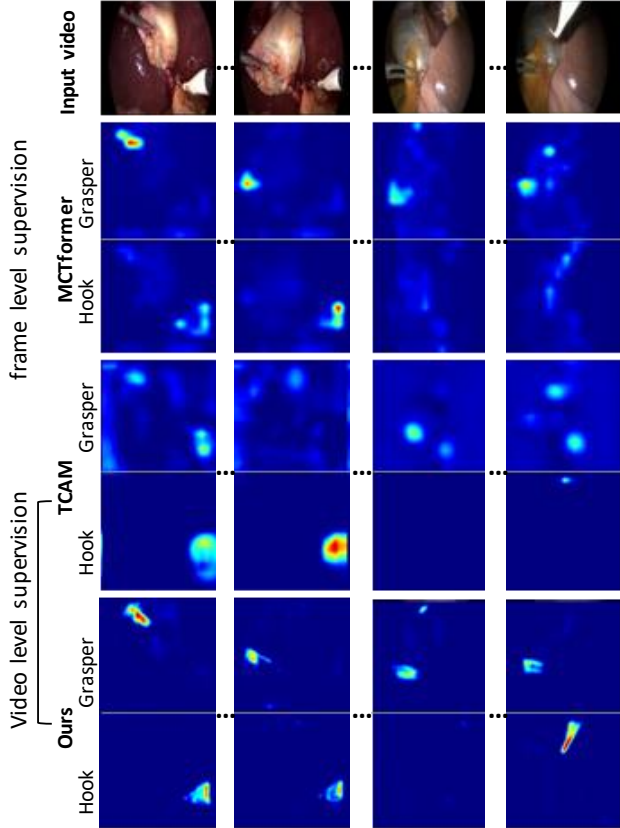


Figure 4. Activation maps of surgical video clips from different methods (MCTformer, TCAM, and our VDST-Net).

full VDST-Net variations. For the surgical video data we utilize another pre-trained Masked Auto-Encoder (MAE) ViT backbone [9] which is tuned on a large scale data for segmentation [18] before it is adapted to the new domain (Cholec80) data.

As presented in Table 2, MCTformer shows the best performance among frame-level supervision methods. Our teacher-only method, also using a transformer encoder but trained on video-level labels, achieves comparable performance thanks to MLP and our spatio-temporal pooling. Full VDST-Net significantly enhances the segmentation performance (61.80% IoU), with a slight trade-off in video classification score due to potential conflicts between KD loss

and classification loss. Figure 4 presents activation maps predicted from different methods, VDST-Net produces activation maps capable of discerning object shapes more effectively than MCTformer.

TCAM achieved commendable video and frame accuracy of 97.08% and 95.10%, respectively. However, in contrast to detection results on the YouTube-Objects data, its segmentation performance drops compared to our method, indicating a challenge in learning representations for WSVOS-TOP problems (i.e. in surgical videos).

4.5. Ablation Study

We evaluated the effects of architecture modifications, pooling variations, and training techniques on model performance (Table 3). Figure 5 shows activation maps from different conditions. Additionally, we demonstrate a further refinement of segmentation generated by using activation maps as prompts for the SAM [18], showcasing a way of generating semantic pseudo-labels.

Importance of knowledge distillation: The results highlight the significance of KD through teacher and student modules for enhanced segmentation accuracy. A standalone student module, lacking frame-level supervision, shows a notable decline in segmentation performance (Dice score from 67.80% to 47.64%), because it predicts error activation by taking information from wrong frames or features, pointed out by red arrowheads in Figure 5. The teacher module has no such issue but lacks the ability to generate activation maps with good connectivity, as indicated by red asterisks in the figure.

Effect of ranked top- k pooling: We investigated the effects of transitioning from ranked top- k pooling to average and max pooling, observing a decline in segmentation performance. Specifically, with average pooling, we noted a decrease in Dice score by 11.49%, and with max pooling, the decrease was 11.71%. Furthermore, there was a considerable decrease in frame classification accuracy, amounting to 3.72% with average pooling and 3.04% with max pooling.

TPC decoupling strategy: Additionally, the proposed

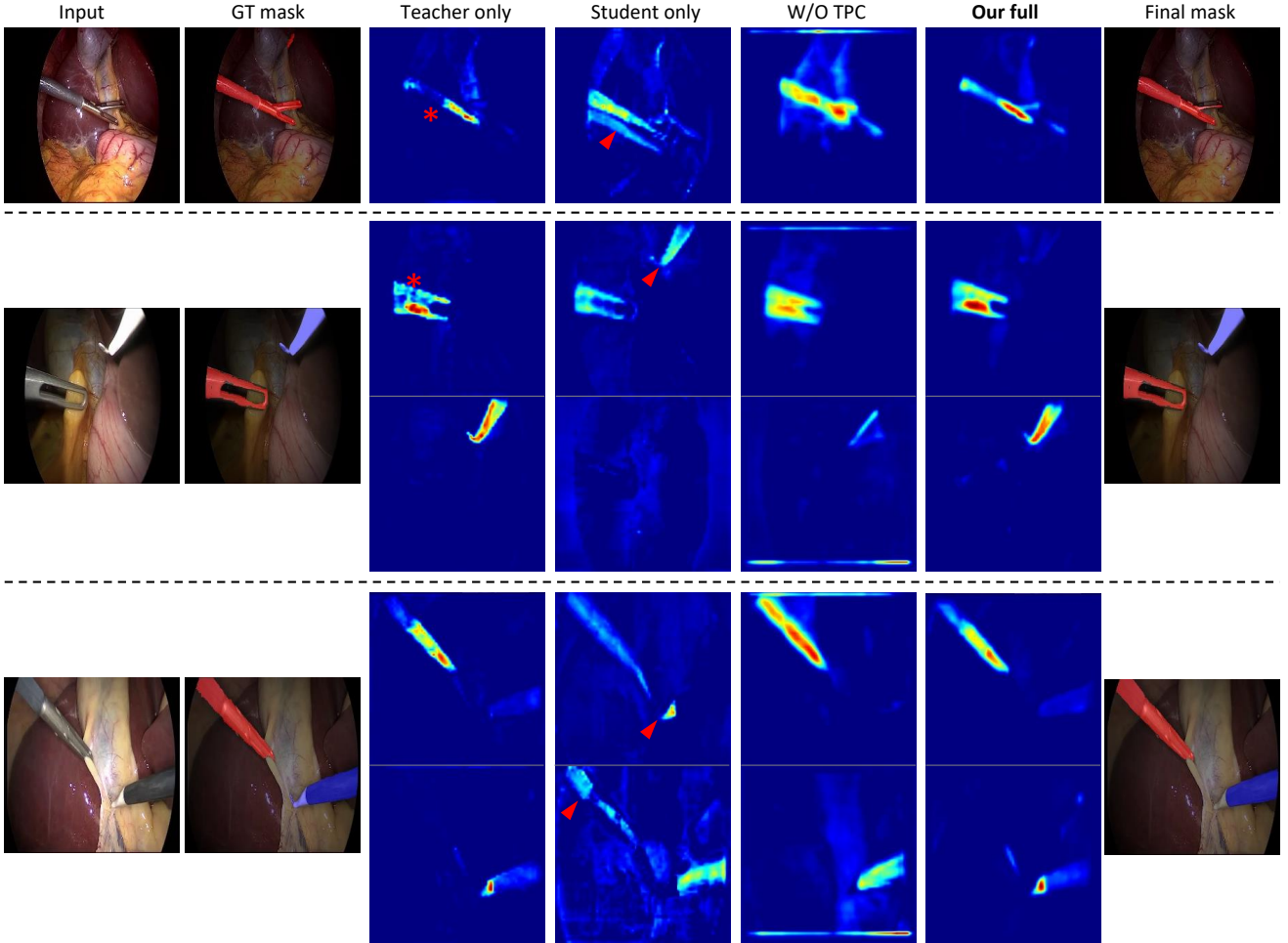


Figure 5. Qualitative results of ablation study and final segmentation masks.

TPC slice kernel for selecting outsignificant activations, enhances the student’s learning. The absence of this component leads to a decline in segmentation performance by 4.16% in Dice and 1.34% in IoU, as demonstrated in Table 3, due to over-introduced loss from non-target class knowledge [52].

5. Conclusion

We presented a novel framework named VDST-Net for WSVOS in surgical videos, which is end-to-end trained with coarse video labels. This method uses a teacher-student architecture and KD to disentangle spatial and temporal knowledge, minimizing temporal interference for the teacher while enhancing the student’s learning capacity. Experiments on both COP and TOP datasets demonstrate our method’s efficacy in generating accurate segmentation maps, outperforming state-of-the-art approaches.

Future work could involve using pseudo masks generated by the student network to train a subsequent

lightweight student network (e.g., U-net) for real-time inference. Additionally, our method could be applied to other video datasets beyond the surgical domain, and exploring spatial knowledge captured by other backbones or foundation models for WSVOS using our method would be interesting. We also suggest that, although the student should not directly update the backbone in a shared backbone design, employing separate backbones combined with continual learning strategies such as Exponential Moving Average (EMA) [39] or Elastic Weight Consolidation (EWC) [19] for updating weights could be beneficial.

6. Acknowledgements.

This work was supported by the University of Pennsylvania Thomas B. McCabe and Jeannette E. Laws McCabe Fellow Award and the Linda Pechenik Montague Investigator Award

References

[1] Soufiane Belharbi, Ismail Ben Ayed, Luke McCaffrey, and Eric Granger. Tcam: Temporal class activation maps for object localization in weakly-labeled unconstrained videos. In *Proceedings of the IEEE/CVF Winter Conference on Applications of Computer Vision*, pages 137–146, 2023. 1, 3, 5, 6

[2] Mathilde Caron, Hugo Touvron, Ishan Misra, Hervé Jégou, Julien Mairal, Piotr Bojanowski, and Armand Joulin. Emerging properties in self-supervised vision transformers. In *Proceedings of the IEEE/CVF international conference on computer vision*, pages 9650–9660, 2021. 6

[3] Ioana Croitoru, Simion-Vlad Bogolin, and Marius Leordeanu. Unsupervised learning of foreground object segmentation. *International Journal of Computer Vision*, 127:1279–1302, 2019. 6

[4] Alexey Dosovitskiy, Lucas Beyer, Alexander Kolesnikov, Dirk Weissenborn, Xiaohua Zhai, Thomas Unterthiner, Mostafa Dehghani, Matthias Minderer, Georg Heigold, Sylvain Gelly, et al. An image is worth 16x16 words: Transformers for image recognition at scale. *arXiv preprint arXiv:2010.11929*, 2020. 3

[5] Ruiqiang Fu, Qingyong Hu, Xiaohu Dong, Yulan Guo, Yinghui Gao, and Biao Li. Axiom-based grad-cam: Towards accurate visualization and explanation of cnns. *arXiv preprint arXiv:2008.02312*, 2020. 6

[6] Tommaso Furlanello, Zachary Lipton, Michael Tschannen, Laurent Itti, and Anima Anandkumar. Born again neural networks. In *International conference on machine learning*, pages 1607–1616. PMLR, 2018. 3

[7] Wei Gao, Fang Wan, Xingjia Pan, Zhiliang Peng, Qi Tian, Zhenjun Han, Bolei Zhou, and Qixiang Ye. Ts-cam: Token semantic coupled attention map for weakly supervised object localization. In *Proceedings of the IEEE/CVF International Conference on Computer Vision*, pages 2886–2895, 2021. 1, 2, 3

[8] Emanuela Haller and Marius Leordeanu. Unsupervised object segmentation in video by efficient selection of highly probable positive features. In *Proceedings of the IEEE international conference on computer vision*, pages 5085–5093, 2017. 6

[9] Kaiming He, Xinlei Chen, Saining Xie, Yanghao Li, Piotr Dollár, and Ross Girshick. Masked autoencoders are scalable vision learners. In *Proceedings of the IEEE/CVF conference on computer vision and pattern recognition*, pages 16000–16009, 2022. 7

[10] Geoffrey Hinton, Oriol Vinyals, and Jeff Dean. Distilling the knowledge in a neural network. *arXiv preprint arXiv:1503.02531*, 2015. 3

[11] W-Y Hong, C-L Kao, Y-H Kuo, J-R Wang, W-L Chang, and C-S Shih. Cholecseg8k: a semantic segmentation dataset for laparoscopic cholecystectomy based on cholec80. *arXiv preprint arXiv:2012.12453*, 2020. 5

[12] Qibin Hou, PengTao Jiang, Yunchao Wei, and Ming-Ming Cheng. Self-erasing network for integral object attention. *Advances in neural information processing systems*, 31, 2018. 2

[13] Rui Hou, Chen Chen, and Mubarak Shah. Tube convolutional neural network (t-cnn) for action detection in videos. In *Proceedings of the IEEE international conference on computer vision*, pages 5822–5831, 2017. 2

[14] Peng-Tao Jiang, Yuqi Yang, Qibin Hou, and Yunchao Wei. L2g: A simple local-to-global knowledge transfer framework for weakly supervised semantic segmentation. In *Proceedings of the IEEE/CVF conference on computer vision and pattern recognition*, pages 16886–16896, 2022. 3

[15] Peng-Tao Jiang, Chang-Bin Zhang, Qibin Hou, Ming-Ming Cheng, and Yunchao Wei. Layercam: Exploring hierarchical class activation maps for localization. *IEEE Transactions on Image Processing*, 30:5875–5888, 2021. 6

[16] Armand Joulin, Kevin Tang, and Li Fei-Fei. Efficient image and video co-localization with frank-wolfe algorithm. In *Computer Vision–ECCV 2014: 13th European Conference, Zurich, Switzerland, September 6–12, 2014, Proceedings, Part VI 13*, pages 253–268. Springer, 2014. 6

[17] Vicky Kalogeiton, Vittorio Ferrari, and Cordelia Schmid. Analysing domain shift factors between videos and images for object detection. *IEEE transactions on pattern analysis and machine intelligence*, 38(11):2327–2334, 2016. 3, 5

[18] Alexander Kirillov, Eric Mintun, Nikhila Ravi, Hanzi Mao, Chloe Rolland, Laura Gustafson, Tete Xiao, Spencer Whitehead, Alexander C Berg, Wan-Yen Lo, et al. Segment anything. *arXiv preprint arXiv:2304.02643*, 2023. 7

[19] James Kirkpatrick, Razvan Pascanu, Neil Rabinowitz, Joel Veness, Guillaume Desjardins, Andrei A Rusu, Kieran Milan, John Quan, Tiago Ramalho, Agnieszka Grabska-Barwinska, et al. Overcoming catastrophic forgetting in neural networks. In *Proceedings of the national academy of sciences*, volume 114, pages 3521–3526. National Acad Sciences, 2017. 8

[20] Yeong Jun Koh, Won-Dong Jang, and Chang-Su Kim. Pod: Discovering primary objects in videos based on evolutionary refinement of object recurrence, background, and primary object models. In *Proceedings of the IEEE conference on computer vision and pattern recognition*, pages 1068–1076, 2016. 6

[21] Alexander Kolesnikov and Christoph H Lampert. Seed, expand and constrain: Three principles for weakly-supervised image segmentation. In *Computer Vision–ECCV 2016: 14th European Conference, Amsterdam, The Netherlands, October 11–14, 2016, Proceedings, Part IV 14*, pages 695–711. Springer, 2016. 2

[22] Philipp Krähenbühl and Vladlen Koltun. Efficient inference in fully connected crfs with gaussian edge potentials. *Advances in neural information processing systems*, 24, 2011. 5

[23] Krishna Kumar Singh and Yong Jae Lee. Hide-and-seek: Forcing a network to be meticulous for weakly-supervised object and action localization. In *Proceedings of the IEEE international conference on computer vision*, pages 3524–3533, 2017. 1, 2

[24] Suha Kwak, Minsu Cho, Ivan Laptev, Jean Ponce, and Cordelia Schmid. Unsupervised object discovery and tracking in video collections. In *Proceedings of the IEEE international conference on computer vision*, pages 3534–3543, 2017. 1, 2

national conference on computer vision, pages 3173–3181, 2015. 6

[25] Hyeokjun Kweon and Kuk-Jin Yoon. From sam to cams: Exploring segment anything model for weakly supervised semantic segmentation. In *Proceedings of the IEEE/CVF Conference on Computer Vision and Pattern Recognition*, pages 19499–19509, 2024. 1, 2

[26] Jungbeom Lee, Eunji Kim, Sungmin Lee, Jangho Lee, and Sungroh Yoon. Ficklenet: Weakly and semi-supervised semantic image segmentation using stochastic inference. In *Proceedings of the IEEE/CVF conference on computer vision and pattern recognition*, pages 5267–5276, 2019. 2

[27] Haofeng Li, Guanqi Chen, Guanbin Li, and Yizhou Yu. Motion guided attention for video salient object detection. In *Proceedings of the IEEE/CVF international conference on computer vision*, pages 7274–7283, 2019. 2

[28] Jianing Li, Shiliang Zhang, and Tiejun Huang. Multi-scale 3d convolution network for video based person re-identification. In *Proceedings of the AAAI conference on artificial intelligence*, volume 33, pages 8618–8625, 2019. 3

[29] Yuqi Lin, Minghao Chen, Wenxiao Wang, Boxi Wu, Ke Li, Binbin Lin, Haifeng Liu, and Xiaofei He. Clip is also an efficient segmenter: A text-driven approach for weakly supervised semantic segmentation. In *Proceedings of the IEEE/CVF Conference on Computer Vision and Pattern Recognition*, pages 15305–15314, 2023. 2

[30] Qing Liu, Vignesh Ramanathan, Dhruv Mahajan, Alan Yuille, and Zhenheng Yang. Weakly supervised instance segmentation for videos with temporal mask consistency. In *Proceedings of the IEEE/CVF Conference on Computer Vision and Pattern Recognition*, pages 13968–13978, 2021. 1, 2

[31] Ze Liu, Jia Ning, Yue Cao, Yixuan Wei, Zheng Zhang, Stephen Lin, and Han Hu. Video swin transformer. In *Proceedings of the IEEE/CVF conference on computer vision and pattern recognition*, pages 3202–3211, 2022. 3

[32] Chinedu Innocent Nwoye, Didier Mutter, Jacques Marescaux, and Nicolas Padoy. Weakly supervised convolutional lstm approach for tool tracking in laparoscopic videos. *International journal of computer assisted radiology and surgery*, 14:1059–1067, 2019. 1, 2

[33] Alessandro Prest, Christian Leistner, Javier Civera, Cordelia Schmid, and Vittorio Ferrari. Learning object class detectors from weakly annotated video. In *2012 IEEE Conference on computer vision and pattern recognition*, pages 3282–3289. IEEE, 2012. 6

[34] Alec Radford, Jong Wook Kim, Chris Hallacy, Aditya Ramesh, Gabriel Goh, Sandhini Agarwal, Girish Sastry, Amanda Askell, Pamela Mishkin, Jack Clark, et al. Learning transferable visual models from natural language supervision. In *International conference on machine learning*, pages 8748–8763. PMLR, 2021. 2

[35] Mrigank Rochan, Shafin Rahman, Neil DB Bruce, and Yang Wang. Weakly supervised object localization and segmentation in videos. *Image and Vision Computing*, 56:1–12, 2016. 6

[36] Alex Sherstinsky. Fundamentals of recurrent neural network (rnn) and long short-term memory (lstm) network. *Physica D: Nonlinear Phenomena*, 404:132306, 2020. 3

[37] Meng Tang, Federico Perazzi, Abdelaziz Djelouah, Ismail Ben Ayed, Christopher Schroers, and Yuri Boykov. On regularized losses for weakly-supervised cnn segmentation. In *Proceedings of the European conference on computer vision (ECCV)*, pages 507–522, 2018. 2

[38] Yu Tian, Guansong Pang, Yuanhong Chen, Rajvinder Singh, Johan W Verjans, and Gustavo Carneiro. Weakly-supervised video anomaly detection with robust temporal feature magnitude learning, 2021. 4

[39] Josh Tobin, Rachel Fong, Alex Ray, Jonas Schneider, Wojciech Zaremba, and Pieter Abbeel. Domain randomization for transferring deep neural networks from simulation to the real world. *arXiv preprint arXiv:1703.06907*, 2017. 8

[40] Pavel Tokmakov, Karteek Alahari, and Cordelia Schmid. Weakly-supervised semantic segmentation using motion cues. In *Computer Vision–ECCV 2016: 14th European Conference, Amsterdam, The Netherlands, October 11–14, 2016, Proceedings, Part IV 14*, pages 388–404. Springer, 2016. 1, 6

[41] Du Tran, Lubomir Bourdev, Rob Fergus, Lorenzo Torresani, and Manohar Paluri. Learning spatiotemporal features with 3d convolutional networks. In *Proceedings of the IEEE international conference on computer vision*, pages 4489–4497, 2015. 3

[42] Yi-Hsuan Tsai, Guangyu Zhong, and Ming-Hsuan Yang. Semantic co-segmentation in videos. In *Computer Vision–ECCV 2016: 14th European Conference, Amsterdam, The Netherlands, October 11–14, 2016, Proceedings, Part IV 14*, pages 760–775. Springer, 2016. 6

[43] Andru P Twinanda, Sherif Shehata, Didier Mutter, Jacques Marescaux, Michel De Mathelin, and Nicolas Padoy. Endonet: a deep architecture for recognition tasks on laparoscopic videos. *IEEE transactions on medical imaging*, 36(1):86–97, 2016. 2, 5

[44] Mikhail Volkov, Daniel A Hashimoto, Guy Rosman, Ozanan R Meireles, and Daniela Rus. Machine learning and coresets for automated real-time video segmentation of laparoscopic and robot-assisted surgery. In *2017 IEEE international conference on robotics and automation (ICRA)*, pages 754–759. IEEE, 2017. 1

[45] Lian Xu, Wanli Ouyang, Mohammed Bennamoun, Farid Boussaid, and Dan Xu. Multi-class token transformer for weakly supervised semantic segmentation. In *Proceedings of the IEEE/CVF Conference on Computer Vision and Pattern Recognition*, pages 4310–4319, 2022. 2, 3, 6

[46] Rongtao Xu, Changwei Wang, Jiaxi Sun, Shibiao Xu, Weiliang Meng, and Xiaopeng Zhang. Self correspondence distillation for end-to-end weakly-supervised semantic segmentation. In *Proceedings of the AAAI Conference on Artificial Intelligence*, volume 37, pages 3045–3053, 2023. 3

[47] Bin Yan, Houwen Peng, Jianlong Fu, Dong Wang, and Huchuan Lu. Learning spatio-temporal transformer for visual tracking. In *Proceedings of the IEEE/CVF international conference on computer vision*, pages 10448–10457, 2021. 3

- [48] Zhiwei Yang, Kexue Fu, Minghong Duan, Linhao Qu, Shuo Wang, and Zhijian Song. Separate and conquer: Decoupling co-occurrence via decomposition and representation for weakly supervised semantic segmentation. In *Proceedings of the IEEE/CVF Conference on Computer Vision and Pattern Recognition*, pages 3606–3615, 2024. 2, 3
- [49] Yazhou Yao, Tao Chen, Guo-Sen Xie, Chuanyi Zhang, Fumin Shen, Qi Wu, Zhenmin Tang, and Jian Zhang. Non-salient region object mining for weakly supervised semantic segmentation. In *Proceedings of the IEEE/CVF conference on computer vision and pattern recognition*, pages 2623–2632, 2021. 2
- [50] Novanto Yudistira, Muthu Subash Kavitha, and Takio Kurita. Weakly-supervised action localization, and action recognition using global-local attention of 3d cnn. *International Journal of Computer Vision*, 130(10):2349–2363, 2022. 1, 2
- [51] Dingwen Zhang, Junwei Han, Le Yang, and Dong Xu. Spftn: A joint learning framework for localizing and segmenting objects in weakly labeled videos. *IEEE Transactions on Pattern Analysis & Machine Intelligence*, 42(02):475–489, 2020. 1
- [52] Borui Zhao, Quan Cui, Renjie Song, Yiyu Qiu, and Jiajun Liang. Decoupled knowledge distillation. In *Proceedings of the IEEE/CVF Conference on computer vision and pattern recognition*, pages 11953–11962, 2022. 3, 4, 8
- [53] Bolei Zhou, Aditya Khosla, Agata Lapedriza, Aude Oliva, and Antonio Torralba. Learning deep features for discriminative localization. In *Proceedings of the IEEE conference on computer vision and pattern recognition*, pages 2921–2929, 2016. 1, 2
- [54] Xiaoyu Zhu, Jeffrey Chen, Xiangrui Zeng, Junwei Liang, Chengqi Li, Sinuo Liu, Sima Behpour, and Min Xu. Weakly supervised 3d semantic segmentation using cross-image consensus and inter-voxel affinity relations. In *Proceedings of the IEEE/CVF International Conference on Computer Vision*, pages 2834–2844, 2021. 3

A. Implementation Details

A.1. Teacher student module details

The teacher and student networks have four layers each. The key difference is that each layer of the teacher network uses an MLP, while the student network uses 3D-CNNs for spatio-temporal convolution. A unique feature of the teacher network is that, to help the backbone learn generalized features at different scales, features from each MLP layer are randomly downsampled during training with a probability of 0.5 before the ranked spatial and temporal pooling. This could be considered a heuristic learning strategy that is close to approaches of randomly masking out feature patches [12,26]. More details about the teacher network's forward operation are shown in the pseudo code in Table S1. As the student uses 3D-CNN instead of MLP, while keeping the overall architecture the same, student's network size and computational load are higher than the teacher's, as presented in Table S2. link to the code: <https://github.com/PCASOLab/VDST-net>.

Table S1. Numpy-like Pseudo-code for teacher branch forward.

```

# image_encoder - ResNet or Vision Transformer
# W_MLP [c_in, c_e]- one layer of proj of the MLP
# W_fc [c_e, N] - learned proj of feature to CAM/Class
# v[bz, d, h, w ,c] - minibatch of videos
# labels[bz, N] - minibatch of ground truth class

# extract feature representations of video
T_f = image_encoder(v) #[bz, d, h_f, w_f, c_f]
T_e = T_f.reshape(bz* d* h_f* w_f, c_e)

for W_MLP in MLP_layers:
    # One layer of MLP
    T_e = ReLU(np.dot(T_e, W_MLP), axis=1)
    # prob 0.5 of downsample
    if Random(0,1) > 0.5:
        T_e.reshape[bz, d, h_new, w_new, c_e]
        # avg pool with kernel k, and stride s
        T_e = Avg_pool_3D (T_e,k=[1,2,2],s=[1,2,2])
        T_e.reshape[bz* d* h_new* w_new* c_e]

    T_e.reshape[bz, d, h_new, w_new, c_e]
    # interpolate in spatial
    T_e = 3D_interpolate (T_e) #[bz, d, h_f, w_f, c_e]
    #ranked spatial pooling
    slice_valid = Rank_pool_hw(T_e,k1) # [bz,d,1,1,c_e]
    #ranked temporal pooling
    final_f = Rank_pool_d(slice_valid,k2) # [bz,1,1,1,c_e]
    final_f.reshape(bz,c_e)

#loss for training
class_logit = sigmoid (np.dot(final_f, W_fc),axis=1)
loss_t = BCE_loss(class_logit, labels, axis=1)
#ST_CAM interface, N class activation maps
T_e.reshape[bz* d* h, w, c_e]
ST_CAM = ReLU(np.dot(T_e, W_fc),axis=1)
ST_CAM.reshape[bz, d, h_f, w_f, N]

```

A.2. Training details

We implemented our training on an Nvidia A5500-based compute platform. Both the teacher and student networks contain a dropout layer after either the MLP (in the teacher)

Table S2. Teacher and student parameter overview with video feature input. FLOPs: Floating-point operations per second.

Parameter	teacher	student
Size	4.02 MB	17.02 MB
Trainable params	1.05 M	4.46 M
Forward/backward pass size	1325.39 MB	2092.8 MB
FLOPs	31.48 G	132.68 G

Table S3. Statistics of the Transient Object Presence (TOP) Cholec80 Data. CholecSeg8K removal: Removal of overlapping clips annotated by CholecSeg8K from the original Cholec80 dataset, as described in section 4.1.

Category	Cholec80		CholecSeg8K removal		
	Frames	Clips	Frames	Clips	FPV
Grasper	102k	5k	83k	4k	63.6%
Bipolar	9k	0.59k	7k	0.48k	48.2%
Hook	103k	4k	87k	3k	80.8%
Scissor	3k	0.24k	3k	0.19k	46.6%
Clipper	6k	0.35k	5k	0.28k	57.0%
Irrigator	10k	0.62k	8k	0.51k	52.7%
Specimen bag	11k	0.62k	9k	0.51k	60.7%

or the 3D-CNN (in the student). For the first nine epochs, only the teacher network was optimized with a dropout rate of 0.5. Subsequently, the student module was enabled with a dropout rate of 0.5, while the teacher's dropout was disabled. After this, both networks were trained for 30 epochs. Optionally, either the teacher or the student can optimize the backbone. For instance, if the teacher is allowed to fine-tune the backbone, the gradient flow from the student to the backbone is stopped.

B. Transient Object Presence Cholec80 Data Statistics

Details of the complete Cholec80 video clips set and the sampled training set are presented in Table S3. Certain instruments, like the Hook, have a high presence frequency throughout the overall dataset or within video. The latter is quantified by the percentage of frames per video (FPV). Instruments such as Scissor and Bipolar appear less frequently, with FPV percentages around or below 60%.

C. Additional Results

Table S4. Results of using separate backbones for teacher and student respectively, CorLoc score on the Youtube-Objects data are reported.

	Full	T only
Res teacher + ViT student	75.0	68.5
ViT teacher + Res student	68.4	63.3

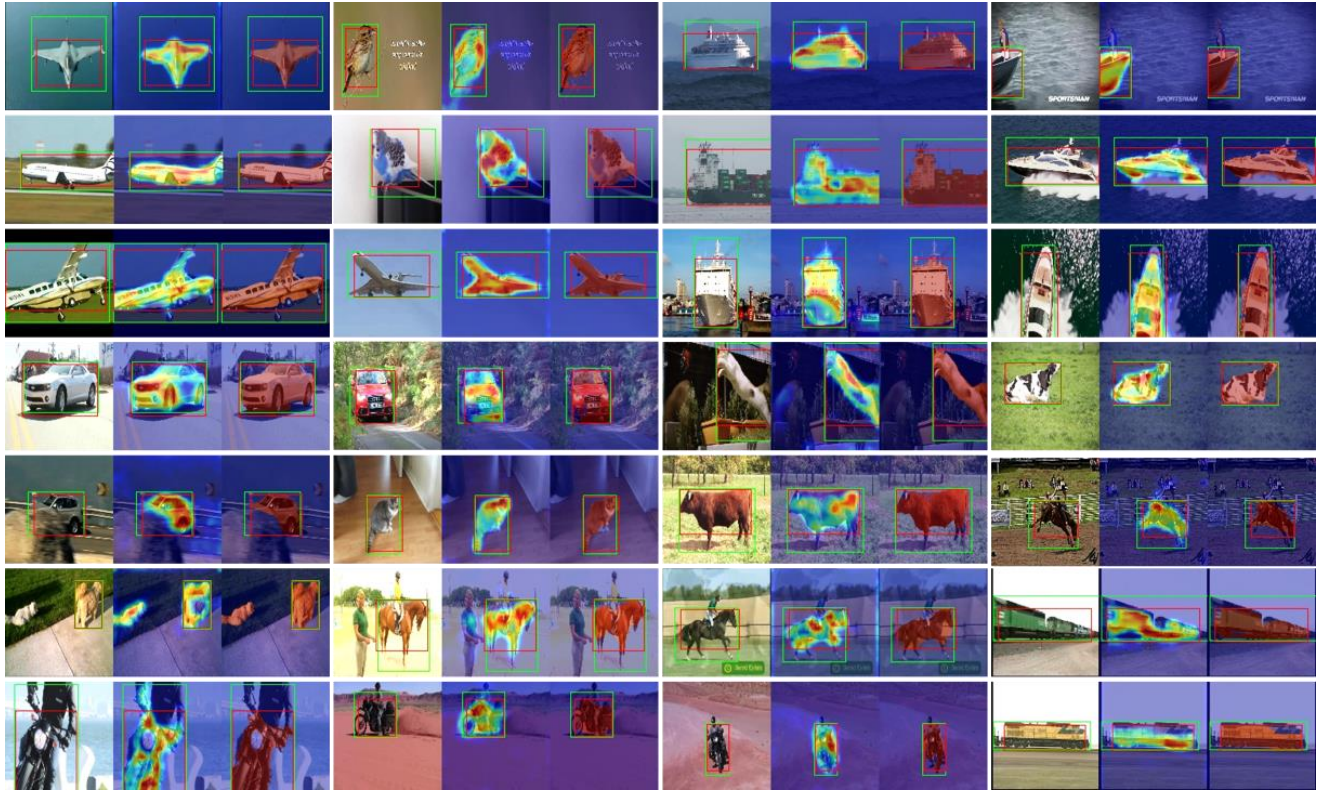


Figure S1. More qualitative results of the proposed method on YouTube-Objects data. Original images, activation maps, and masks after thresholding are presented sequentially. Our method demonstrates robustness, producing activation maps and segmentation masks that accurately follow the objects' contours, with minimal false activation on the background.

Table S5. Results of using Resnet34 as feature extractor on Cholec80 data.

	IoU[%] \uparrow	Dice[%] \uparrow	HD[pix] \downarrow
VDST-Net	43.58	46.15	53.50

We also present results using a ViT backbone for the student and a ResNet backbone for the teacher, as well as the reverse configuration. As shown in Table S4, both configurations improve performance over the teacher alone. Notably, using ViT as the student results in the highest performance among them.

Additionally, we utilize a ResNet-34 backbone for the TOP cholec80 videos (Table S5). While this approach shows a decline in accuracy compared to our ViT-based method, it still achieves comparable performance to other state-of-the-art methods, as presented in Table 2.

More qualitative results on the YouTube-Objects dataset are presented in Figure S1.